Available online at www.sciencedirect.com
SCIENCE DIRECT®
Journal of Nuclear Materials 343 (2005) 262–266
journal of nuclear materials
www.elsevier.com/locate/jnucmat

Microstructural study of EC316LN and its welds irradiated in SINQ target-3

D. Hamaguchi *, Y. Dai

Spallation Neutrion Source Division, PSI, CH-5232 Villigen PSI, Switzerland

Abstract

Solution-annealed (SA) austenitic stainless steel EC316LN and its welds were irradiated in SINQ Target-3. The irradiation dose was up to 11 dpa and the temperature ranged from around 70 °C to 350 °C. For the SA metal, TEM investigations show that the main features of irradiation damage for the SA metal are high-density small black dot defects and large Frank loops. The density and size of the small dot defects are independent of irradiation dose with a mean size of about 1.2 nm and a density of about 4.5×10^{23} m^{-3}. The density of Frank loops also varies little with dose, while the size increases with dose. No bubbles or voids were found in specimens irradiated up to 9.3 dpa at below 290 °C, while high-density small bubbles were observed in the specimens irradiated to 11 dpa at 350 °C. For the welds metal (namely in the fusion zone), the main features are the same, high-density small defect clusters and large Frank loops formed after irradiation. However, high-density small bubbles were observed in a specimen irradiated to 10 dpa at a temperature of around 290 °C.

1. Introduction

Since the neutron irradiation response of type 316LN stainless steel is generally well understood, it is a candidate for the structural material to support the liquid target of future high-energy spallation neutron sources and accelerator driven systems. In a high-power spallation target, however, the beam window and other components exposed in high-energy proton beam will be subjected to much higher helium production rate compared to materials in a fission or fusion irradiation environment. In a spallation target environment, the helium production rate in terms of He/dpa is 10–100 times higher than that of neutron irradiation. Therefore, it is of essential importance to study the change in material properties and microstructure of materials irradiated in a spallation target environment and to establish a necessary material database for application to a spallation neutron source.

For the target structural material in a spallation neutron source, weld structure cannot be avoided in the irradiation zone. Therefore, it is necessary to understand the behavior of weld metals in such an environment. In the present study, the microstructure of EC316LN and its weld metal, which were irradiated in SINQ Target-3 for the first SINQ target irradiation program, have been investigated to understand the change in microstructure in these materials after irradiation.

* Corresponding author. Tel./fax: +81 29 287 8992.
E-mail address: hamadai@tokai.t.u-tokyo.ac.jp (D. Hamaguchi).

0022-3115/$ - see front matter © 2005 Published by Elsevier B.V.
doi:10.1016/j.jnucmat.2004.12.013

2. Experimental procedure

The first SINQ target irradiation program (STIP-1) was done in SINQ Target-3 between 1998 and 1999. The target received a total of 6.8 Ah proton charge with beam energy of 560 MeV. The specimens, including 3 mm-diameter TEM disks, were irradiated in special rods, which were placed in the heavy irradiation zone of the target. More details of the STIP-1 experiment were previously reported [1]. The materials chosen for this study are solution annealed (SA) EC316LN and its tungsten-inert-gas (TIG) welds. The composition of the EC316LN is listed in Table 1. The information on TIG weld processing is listed in Table 2. TEM disks (3 mm-diameter) of the two materials were irradiated at different positions. The irradiation doses ranged from 2.2 to 11 dpa and the temperature was from around 70 to 350 °C. The irradiation conditions and the calculated and measured helium and hydrogen concentration of the samples are listed in Table 3. It can be seen that the measured helium concentrations are higher while the measured hydrogen concentrations are much lower than calculated values. The detail information and discussion can be found in Ref. [2]. In this table, J-series represent the SA metal and E-series represent the TIG weld metal. After irradiation, the samples were electropolished in a twinjet Tenupol unit, and the microstructure was examined with a JEOL-2010 TEM operating at 200 kV.

Table 1
Chemical composition of the EC316LN

Fe	Cr	Ni	Mo	Mn	C	Si	P	S	N
Bal	17.45	12.2	2.5	1.81	0.024	0.39	–	–	0.067

Table 2
Weld procedure for the TIG weld

	TIG weld
Plate thickness	6 mm
Beam energy	10–12 V
Beam current	65–75 mA
Welding rate	25 mm/min

3. Results

3.1. Microstructure in EC316LN SA metal

The microstructure of the unirradiated material is shown in Fig. 1. The main feature of the microstructure for the unirradiated material is a relatively low density of network dislocations. The dislocation density is about 1.8×10^{13} m^{-2}. It can also be noted that the densities of carbides and other precipitate are low.

After irradiation, a high-density Frank loops and small dot defects were introduced. Fig. 2 shows the microstructure of each specimen after irradiation. Measured density and mean size of dot defects, Frank loops and bubbles are listed in Table 4. The density of both loops and dot defects do not change significantly in samples J2, J9, and J6, where the dose varies from 2.2 to 9.3 dpa and the irradiation temperature changes from about 70 to 286 °C respectively. However, in sample J1 which was irradiated to 11 dpa at about 350 °C, the density of both loops and dot defects are about half of the other three samples. The mean size of the dot defects

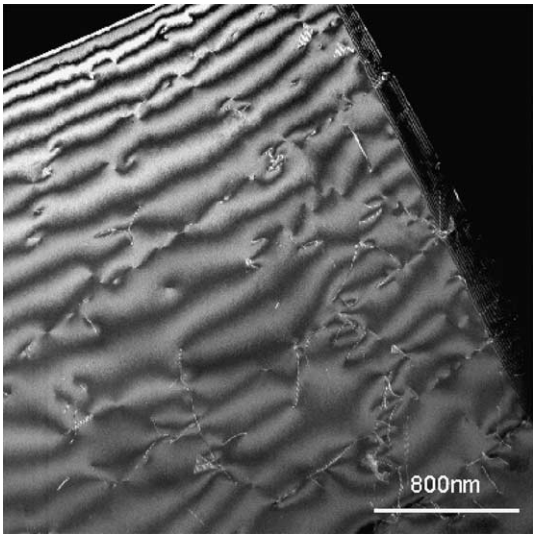

Fig. 1. The microstructure in the unirradiated SA metal.

Table 3
Irradiation conditions of the specimens

Sample	Dose (dpa)	Irradiation temperature (°C)	He (cal.) (appm)	He (meas.) (appm) ± 1%	H (cal.) (appm)	H (meas.) (appm) ± 24%
J2	2.2	68 ± 8	109	139	880	390
J9	5.8	208 ± 18	320	–	2336	–
J6	9.3	286 ± 22	498	707	4033	320
J1	11	353 ± 28	730	–	5036	–
E4	5.5	196 ± 16	300	–	2216	–
E23	10	293 ± 23	579	–	4438	–

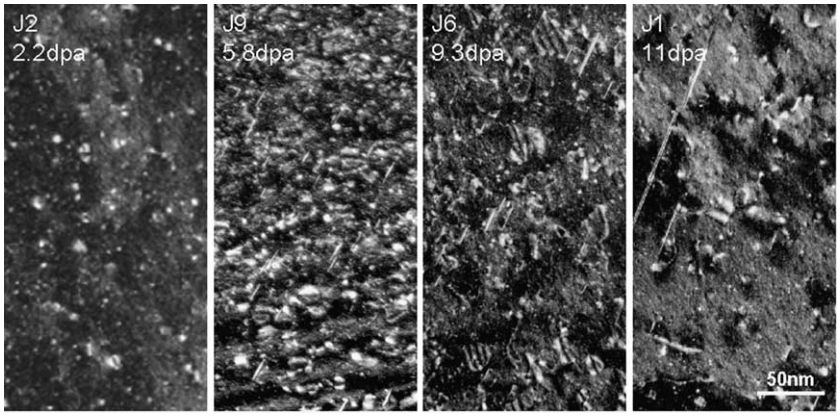

Fig. 2. The microstructure in SA metal after irradiation. J2, J9, J6 and J1 correspond to the specimens irradiated at different conditions as listed in Table 4. The image taken near [1 1 0] zone axis with $g = 200$.

Table 4
Measured density and mean size of the defects after irradiation

Sample	Dot defects		Frank loops		Bubbles	
	Mean size (nm)	Density ($\times 10^{23}$ m^{-3})	Mean size (nm)	Density ($\times 10^{23}$ m^{-3})	Mean size (nm)	Density ($\times 10^{23}$ m^{-3})
J2	1.2	4.7	4.5	1.4	–	–
J9	1.1	4.1	10.2	1.1	–	–
J6	1.4	4.6	12.4	1.2	–	–
J1	1.8	2.1	15.9	3.6×10^{22}	1.6	5.3
E4	1.5	4.3	13.5	4.1×10^{22}	–	–
E23	1.1	2.2	12.2	2.6×10^{22}	1.9	1.8

does not show a significant difference either, while the mean size of the loops shows a constant increase with dose. In sample J1, a new feature of irradiation damage was also observed. High-density bubbles with a mean size of around 1.6nm were observed, as is shown in Fig. 3. The bubble density is about 5.3×10^{23} m^{-3}. The bubbles are distributed nearly homogeneously inside grains and there is no evident bubble segregation at grain boundaries. It can also be noted that there was no denuded zone for the bubbles near grain boundaries.

3.2. Microstructure in EC316LN TIG weld metal

Fig. 4 shows the microstructure of the TIG weld metal before irradiation. The main feature of the microstructure is a relatively small density of dislocation lines, about 3.7×10^{13} m^{-2}, which is about two times of that in the SA metal. It can also be noted that there are a lot of carbides and δ-ferrite along grain boundaries.

Fig. 5 shows the microstructure after irradiation. The irradiation also introduced a high density of Frank loops and small dot defects in the TIG weld metal, as is the case of the SA metal. Although the mean size of loops is similar, the density of the loops in TIG weld

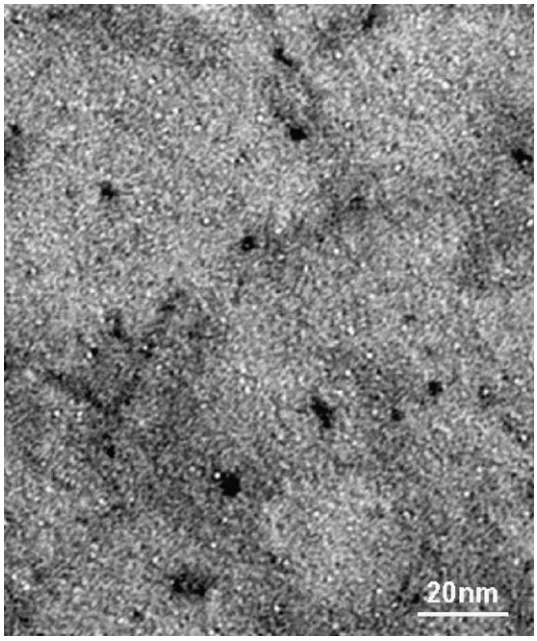

Fig. 3. The bubble image in the sample J1 after irradiation to 11 dpa at 353 °C.

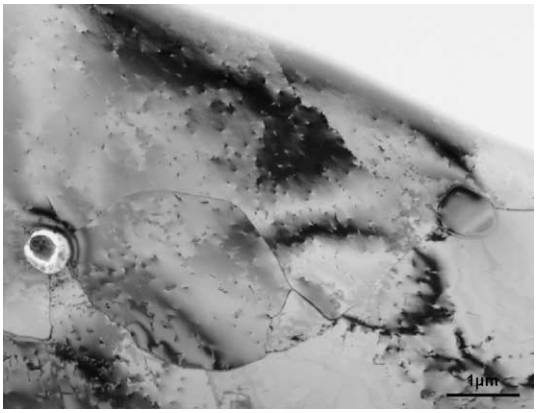

Fig. 4. The microstructure in the unirradiated TIG weld metal.

metal was less than half of that of the SA metal irradiated at a similar irradiation condition. For the dot defects, on the other hand, the density and size do not show much difference from those of the SA metal. Measured density and size of the defects in TIG weld material is also listed in Table 4.

High-density small bubbles were also observed in the TIG weld metal irradiated to about 10 dpa at 293 °C (sample E23), as shown in Fig. 5. The density is about 1.8×10^{23} m^{-3}, and the mean size is about 1.9 nm. The bubbles are distributed nearly homogeneous inside grains and no grain boundary bubble segregation was observed.

It can also be noted that inside δ-ferrite, the defect formation was much slower compared to the adjacent austenitic grains, as can be seen in Fig. 5. In sample E4, where the dose level is about 5.5 dpa, almost no defect formation was observed. Even in sample E23, which received a higher dose of about 10 dpa, the defect density is much lower compared to the austenitic grains. There was also a large denuded zone of about 250 nm observed in δ-ferrite region in sample E23.

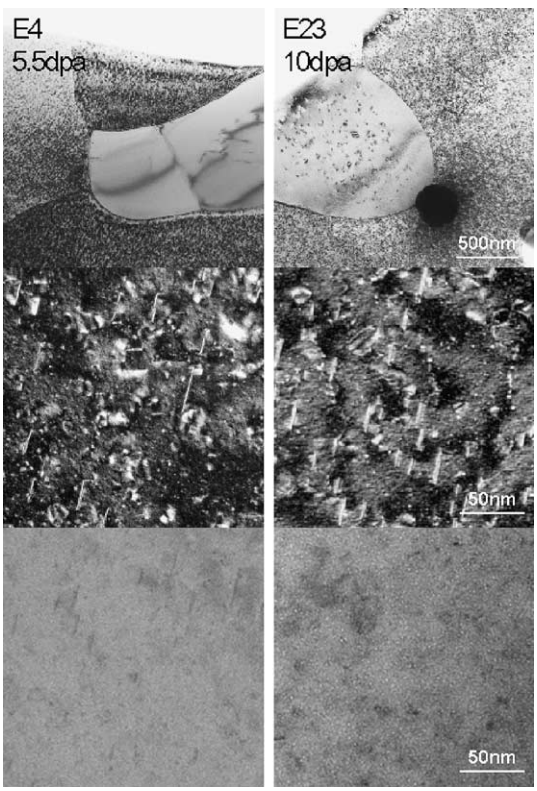

Fig. 5. The microstructure after irradiation in the TIG weld metal. E4 and E23 correspond to the specimens listed in Table 4.

4. Discussion

The typical microstructure under irradiation in austenitic stainless steels consists of dislocation loops, network dislocations, cavities, and precipitates. However, a pronounce change in microstructural evolution occurs as a function of irradiation temperature. In the lower temperature regime, where irradiation temperature is below 300 °C, the dominant microstructural features in austenitic steels are faulted dislocation loops and dot defects [3]. The microstructural behavior of EC316LN in the present study shows relatively good agreement with neutron irradiation studies [4–10]. In SA metal irradiated below 300 °C in this study (sample J2, J9 and J6), the main features are also a high-density dislocation loops and small dot defects. However, the number density of the defects is a little higher compared to neutron irradiation. A higher number density of the defect produced under high-energy proton irradiation as compared to neutron irradiation case was also reported for 304L stainless steel [11]. This might be due to the high helium production rate induced by high-energy proton irradiation, since a high concentration of helium can stabilize the formation of vacancy clusters [12].

High-density small bubbles were also observed in the SA metal in this study irradiated above 300 °C (sample J1). This result also agrees with former mixed spectrum neutron irradiation experiment in HFIR, where high-density small bubbles formed after irradiation at around 300 °C [6,7]. The measured density and size of bubbles in this study are also consistent with the HFIR irradiation results.

Generally, pronounced cavity formation occurs in stainless steels at higher temperatures above 300 °C. However, in the TIG weld metal of this study, the

bubble formation was observed at a lower irradiation temperature, 293 °C. the reason for the difference is not clear. More systematic studies are needed.

5. Conclusion

Detailed TEM observations were performed on solution-annealed EC316LN and its TIG weld metal irradiated in SINQ Target-3 to investigate the microstructural evolution in a spallation neutron source irradiation environment. In SA metal, the microstructural evolution showed that the dominant defect structure in the samples irradiated at temperature below 300 °C is high-density small dot defects and Frank loops. In the sample irradiated at 350 °C, high-density small bubbles were also observed. In the TIG weld metal, the dominant microstructure after irradiation is also high-density dot defects and loops. However, in TIG weld metal, high-density small bubbles were observed in a sample irradiated at around 290 °C.

References

[1] Y. Dai, G.S. Bauer, J. Nucl. Mater. 296 (2001) 43.
[2] Y. Dai, Y. Foucher, M.R. James, B.M. Oliver, J. Nucl. Mater. 318 (2003) 167.
[3] S.J. Zinkle, P.J. Maziasz, R.E. Stoller, J. Nucl. Mater. 206 (1993) 266.
[4] P.J. Maziasz, J. Nucl. Mater. 191–194 (1992) 701.
[5] P.J. Maziasz, Trans. ANS 39 (1981) 433.
[6] S. Hamada, M. Suzuki, P.J. Maziasz, A. Hishinuma, M.P. Tanaka, Effects of radiation on materials, vol. 1, ASTM STP 1046, in: N.H. Packan, R.E. Stoller, A.S. Kumar, (Eds.), 1989, p. 172.
[7] M.P. Tanaka, S. Hamada, A. Hishinuma, P.J. Maziasz, J. Nucl. Mater. 155–157 (1988) 801.
[8] T. Muroga, Y. Miyamoto, H. Watanabe, N. Yoshida, J. Nucl. Mater. 155–157 (1988) 810.
[9] N. Yoshida, J. Nucl. Mater. 174 (1990) 220.
[10] N. Hashimoto, E. Wakai, J.P. Robertson, J. Nucl. Mater. 273 (1999) 95.
[11] Y. Dai, X. Jia, J.C. Chen, W.F. Sommer, M. Victoria, G.S. Bauer, J. Nucl. Mater. 296 (2001) 174.
[12] R.E. Stoller, J. Nucl. Mater. 174 (1990) 289.